IMPROVED FORMATION EVALUATION THROUGH IMAGE-DERIVED DENSITY

R. J. Radtke,[1] R. A. Adolph,[2] H. Climent,[1] L. Ortenzi,[3] N. Wijeyesekera[4]

[1]Schlumberger, Sugar Land Product Center, Sugar Land, Texas
[2]Schlumberger, Princeton Technology Center, Princeton, New Jersey
[3]Schlumberger Oilfield Services, Stavanger, Norway
[4]Schlumberger Technical Services, Dubai, United Arab Emirates

ABSTRACT

Logging while drilling (LWD) is a challenging environment in which to make a formation density measurement. The measurement is strongly affected by tool motion and is influenced by the drilling fluid composition. The net effect is formation density and photoelectric factor (Pe) measurements that can be inaccurate or misleading.

The accuracy of the measurements can be greatly improved by acquiring data in both depth and azimuthal dimensions, assembling these data into a two-dimensional image, and selecting the density measurements least influenced by borehole effects from this image. In LWD, azimuthal data are acquired most economically from one set of sensors swept around the borehole by the rotation of the drillstring. Selection of the density measurements is then accomplished in three steps. First, a quality factor is computed for each depth and azimuthal sector. This quality factor is largest when the density measurement is indicated to be closest to the formation density. Second, the centroids of the high-quality regions are computed. The set of these centroids as a function of depth is called the tool path. Third, density and Pe measurements are calculated from the sectors along the tool path. In many cases, the path lies along the bottom of the borehole, and the bottom-quadrant density is the highest-quality density.

By construction, this algorithm yields the highest-quality density and Pe measurements possible. This technique has several other advantages: it is computed only from density sensor data, it is immune to the statistical bias and limited applicability of maximum-density approaches, and the tool path serves as a powerful quality-control indicator.

This paper describes the image-derived density algorithm and presents several examples demonstrating its usefulness. The algorithm is shown to compensate for shifts and erratic motion of the LWD tool. Interpretation problems solved by the image-derived density technique are also discussed.

INTRODUCTION

Formation density measurements are required to be accurate to a level of 0.01 g/cm^3, and this poses a significant challenge for density tool design and algorithm development. Conventional density tools send gamma rays into a formation and record the rate at which they are reflected back to its detectors (for a review, see Ellis, 1987, and references therein). The count rates can be directly related to formation density when the tool is in a reference condition with respect to the borehole, which typically is when the tool is in direct contact with the formation. During logging, the density tool is usually stood off from the formation and the gap is filled with either mudcake or drilling fluid, which degrades the accuracy of the measurement. The standard method of correcting for this effect is to make a compensated density measurement using two gamma ray detectors, a short-spaced and a long-spaced one, and analyzing the measured count rates within a spine-and-ribs framework. This approach satisfies the demanding accuracy specifications when the standoff is relatively small, the mud is relatively light, or both conditions.

To ensure that the density tools are operated within the regime in which the spine-and-ribs approach is accurate, additional actions must be taken. In wire-line (WL) logging, the density tool's source and detectors are usually mounted on an articulated pad that is pressed against the formation. In LWD, this configuration is not possible. Instead, a stabilizer can be placed on the outside of the drill collar to reduce the effective standoff between the tool and the formation (Figure 1a). For reasons related to the drilling process, the stabilizer diameter usually must be significantly less than the bit size (undergauge) or absent entirely (Figure 1b). In these situations, the spine-and-ribs approach does not yield an accurate density for all orientations of the tool, but it can yield accurate densities for some of

them. In particular, in deviated sections, gravity tends to pull the density tool to the bottom of the borehole. The density measurements made when the detectors face the bottom of the hole are then the most accurate.

The availability of these orientation-dependent density measurements is a unique feature of the LWD environment. In WL logging, the contact point of the density pad with the borehole wall is neither fixed nor often known. In ovalized boreholes, the contact point is often in the long axis of the wellbore, but the best density may be obtained from a contact point in the short axis. Although it is possible to include multiple detector pads and the appropriate sensors to provide density data from multiple directions, it has not been economically feasible. In LWD, the rotation of the drillstring—and hence of the density tool—allows a single set of detectors to sweep through all orientations around the borehole. With the addition of a set of magnetometers to the density tool and use of the known properties of the well trajectory and local magnetic field, the density measurements can be acquired as a function of both depth and azimuthal orientation (Evans *et al.*, 1995; Carpenter *et al.*, 1997). This capability has been available in, for example, the adnVISION* Azimuthal Density Neutron Vision tools for many years.

The azimuthal binning scheme used in these tools and this paper is shown in Figure 1a. The borehole is divided into 16 azimuthal sectors, each sector representing a 22.5° slice of the borehole's circumference. As the tool rotates, each count observed in each gamma ray detector is added to the bin corresponding to the tool's orientation at the time it was detected. After a pre-set interval, on the order of 10 s, the contents of the bins are converted to count rates and recorded as a function of the acquisition time. The azimuthal bins are then zeroed, and the process repeated. At the surface, the time-based data can then be converted into depth-based data.

The resulting two-dimensional data can be thought of as an image. The character of the image reflects the immediate surroundings of the density tool when the measurements were made and is one of the single best quality-control indicators available. For an in-gauge stabilized density tool in good hole conditions, the density measurements are accurate around the entire circumference of the borehole. As shown in Figure 1c, the resulting image gives a full picture of the borehole, from which it is straightforward to extract information about formation bed thickness, strike, and dip. The example shown in Figure 1c is from a nearly horizontal well, so the bedding planes intersect the wellbore at high apparent dip angles. When viewed as a two-dimensional image, this produces the chevron-shaped features apparent in the figure.

For undergauge stabilized or slick density tools, the standoff between the tool and the borehole can greatly exceed that correctable by spine-and-ribs algorithms along certain directions. As seen in Figure 1d, the resulting image typically has a band of good-quality formation density measurements at the bottom of the hole surrounded by a featureless region at the top of the hole representing the poor-quality density measurements. The well in this example is only inclined 25° from the vertical. As a result, bedding planes intersect the wellbore at low apparent dip angles, and the chevron-like features seen in Figure 1c are absent. Because of the presence of washouts or borehole ovalization, even in-gauge stabilized tools can display images similar to that of Figure 1d.

Along with the desirable rotation, LWD tools are also prone to many other motions that are less advantageous. These motions can dynamically change the azimuthal orientation along which the highest-quality formation density measurements are made. An example is shown in Figure 2. Figure 2a presents a cross section of a slick tool in a deviated borehole in its typical position: gravity has pulled the tool to the bottom of the borehole, and the bottom-directed measurements provide the highest-quality densities. In Figure 2b, friction between the borehole wall and some part of the drillstring has caused the tool to "climb up" the right-hand side of the borehole. The highest-quality formation densities are no longer obtained from the bottom-directed measurements but rather from those made between the bottom and right directions.

There are other reasons that the azimuthal location of the highest-quality measurements may change. For example, the drillstring may push portions of the tool away from the bottom of the borehole when building or dropping angle or changing azimuth. The same effect can be achieved through unintentional variation of the borehole trajectory resulting from mechanical instabilities in the drillstring. An extreme example of this effect is the corkscrewed or threaded borehole (Carpenter *et al.*, 1997). Outside of the drillstring itself, the borehole may also display washouts, ovalization, breakouts, or fractures along particular directions.

* Mark of Schlumberger

This paper describes an algorithm that can compensate for many drilling effects in an LWD density tool (Radtke *et al.*, 2001). The algorithm uses the azimuthal information in the images to select the measurements that yield the highest-quality formation density measurements. The selection process occurs in three stages. In the first, a quality factor is computed for each depth and azimuthal sector. The quality factor is largest when the density measurement is indicated to be closest to the formation density. In the second, the centroids of the high-quality regions are computed. The set of these centroids as a function of depth is called the tool path. Finally, density and Pe measurements are calculated from the four sectors centered on the tool path. In many cases, the tool path lies along the bottom of the borehole, and the bottom-quadrant density is the highest-quality measurement.

This procedure is referred to as IDD* Image-Derived Density. In the next section, the IDD algorithm is described in detail. Several examples are presented to illustrate the versatility of this approach and some of the interpretation problems that can be solved by using it.

ALGORITHM

The IDD algorithm uses the compensated density image to compute a single compensated density. It identifies which sectors at each depth level provide the highest-quality measurements and computes a density measurement based on those sectors. It essentially automates what a skilled log analyst does when interpreting a density image.

The algorithm consists of three steps:

1. *Quality factor computation.* For each depth level and sector, the short- and long-spaced densities and volumetric photoelectric factor are used to compute a quality factor. The quality factor is based on qualitative expectations and an empirical choice of parameters. Larger quality factors represent more accurate density measurements.
2. *Tool path identification.* As a function of depth, the centroid of the region of high-quality measurements defines a tool path. The tool path can be thought of as the path of closest approach of the tool to the formation. This path is computed from the quality factor at each depth level by a partial Fourier decomposition.
3. *Density calculation.* The density is computed at each depth level by averaging the bulk density over four sectors centered on the tool path. Fractional sectors are accounted for by linear interpolation.

These steps are next described in detail.

Quality factor computation. The quality factor is inspired by the spine-and-ribs approach, in which high-quality points lie near the spine. Consequently, it is parameterized by the apparent densities along and normal to the spine. In this paper, the azimuthal data are binned into 16 sectors with the sector boundaries as indicated in Figure 1a. If these sectors are indexed by $\alpha = 0, 1, 2, \ldots, 15$, then at depth level i, the apparent density along the spine is defined as

$$\rho_{i\alpha}^{\parallel} = \rho_{i\alpha}^{LS} \tag{1}$$

and that normal to the spine as

$$\rho_{i\alpha}^{\perp} = \rho_{i\alpha}^{LS} - \rho_{i\alpha}^{SS} . \tag{2}$$

Here, $\rho_{i\alpha}^{LS}$ and $\rho_{i\alpha}^{SS}$ are the measured long- and short-spaced electron density indices. An electron density index ρ_e is obtained from a bulk density ρ_b by

$$\rho_e = (\rho_b + 0.1883)/1.0704 \tag{3}$$

(Ellis, 1987). In addition, the apparent volumetric photoelectric factor $U_{i\alpha}$ is used to indicate when the measured density is contaminated by high-Pe mud.

The quality factor $Q_{i\alpha}$ at depth level i in sector α is defined as a product of a spine, rib, and U factor:

$$Q_{i\alpha} = F_{Spine}(\rho_{i\alpha}^{\parallel}) \times F_{Rib}(\rho_{i\alpha}^{\perp}) \times F_U(U_{i\alpha}). \tag{4}$$

The functions making up the quality factor are slightly tool-dependent, but have the generic forms presented in Figure 3. As seen in Figure 3a, the spine factor associates high-quality measurements with readings in the range of formation densities. It excludes low densities, which are more characteristic of the drilling fluid, and high densities, which are unphysical. The rib factor (Figure 3b) connects high-quality measurements with small $\left|\rho_{i\alpha}^{\perp}\right|$. In the spine-and-ribs algorithm, $\rho_{i\alpha}^{\perp}$ is related to the correction applied to the long-spaced density to yield the compensated density, usually referred to as "delta-rho." Selecting small $\left|\rho_{i\alpha}^{\perp}\right|$ thus corresponds to situations that have generally low standoff and correctable mud-weight effects. The U factor (Figure 3c) indicates high quality only when the measured U is close to values expected for a formation. Higher or lower values suggest that the measurement is contaminated by mud effects and is therefore of lower quality. The boundary between high- and low-quality regions of apparent U is blurred due to the uncompensated nature of the U measurement. Consequently, the range of acceptable U values shown

in Figure 3c is slightly larger than those of true formations.

Tool path identification. Intuitively, the tool path at a given depth level is the centroid of the high-quality-factor region at that level. To make this idea quantitative and to reduce the effect of statistical noise, the centroid is obtained from a low-order Fourier expansion.

Specifically, a continuous function of the azimuthal angle θ, $\tilde{Q}_i(\theta)$, is constructed from the discrete $Q_{i\alpha}$ by using

$$\tilde{Q}_i(\theta) = a_{i0} + a_{i1}\cos(\theta) + b_{i1}\sin(\theta), \quad (5)$$

where the Fourier coefficients are given by

$$a_{il} = \frac{1}{16}\sum_{\alpha=0}^{15}\cos(l\theta_\alpha)\,Q_{i\alpha}, \quad l = 0,1, \quad (6)$$

and

$$b_{i1} = \frac{1}{16}\sum_{\alpha=0}^{15}\sin(\theta_\alpha)\,Q_{i\alpha}, \quad (7)$$

and $\theta_\alpha = (2\alpha+1)\pi/16$ is the angle in radians of the center of sector α. Although this function does not reproduce $Q_{i\alpha}$ exactly, its maximum is a reasonable estimate of the "center" of the high-quality region. The tool path at depth level *i*, θ_i^{path}, is then

$$\theta_i^{path} = \tan^{-1}(b_{i1}/a_{il}), \quad (8)$$

with $0 \le \theta_i^{path} < 2\pi$.

According to this definition, the tool path is a continuous variable. It forms the basis for the density calculation and can be plotted on a density or Pe image. This visualization is a powerful quality-control tool. By examining where the tool path falls on the density, delta-rho, Pe, or quality factor images, the log analyst has instant qualitative feedback on the appropriateness of the choice of path and of the resulting density.

Density calculation. The image-derived density is computed by averaging the sectors of the compensated density image that are within in ±2 sectors of the tool path. For the definition of sectors used in this paper and shown in Figure 1a, this amounts to ±90° or ±π/2 radians.

At each depth level *i*, the image-derived density, ρ_i^{IDD}, is computed from the compensated density image $\rho_{i\alpha}$ and the tool path by a simple weighted average:

$$\rho_i^{IDD} = \sum_\alpha w_{i\alpha}\rho_{i\alpha} \Big/ \sum_\alpha w_{i\alpha}. \quad (9)$$

Here, the weight $w_{i\alpha}$ depends on θ_i^{path} and is equal to the fraction of sector α, defined as the angular interval $[\alpha\pi/8, (\alpha+1)\pi/8]$ that lies within the interval $\left[\theta_i^{Path} - \pi/2, \theta_i^{Path} + \pi/2\right]$. That is, the weight is unity if sector α lies entirely within the interval of two sectors from the tool path, zero if it lies entirely outside this interval, and the fraction of the sector that overlaps this interval in the intermediate cases. The continuous tool path and fractional weighting of some sectors prevent unphysical discontinuities in ρ_i^{IDD} resulting from sector-sized jumps in the tool path that would otherwise occur.

In the same manner as for the density, image-derived delta-rho and volumetric photoelectric factors can be computed. An image-derived Pe can then be obtained from the image-derived density and volumetric photoelectric factor in the usual way (Ellis, 1987).

EXAMPLES

By their construction, the image-derived density and Pe are the highest quality that can be obtained from a given set of measurements interpreted within a spine-and-ribs algorithm. As mentioned in the "Introduction," in most cases these highest-quality measurements lie along the bottom of the borehole. In examining the effectiveness of the IDD algorithm, it is therefore instructive to make comparisons to the bottom-quadrant density,

$$\rho_i^{Bottom} = \frac{1}{4}\sum_{\alpha=6}^{9}\rho_{i\alpha}. \quad (10)$$

This section presents this comparison for several examples.

Experience has shown that the IDD algorithm is effective for nearly all tool and hole sizes. It is most useful when the stabilizer diameter is much less than the bit size and the borehole is deviated. For this reason, most of the examples here are taken from deviated 12¼-in. boreholes logged by adnVISION825* Azimuthal Density Neutron Vision 825 tools, which are slick 8.25-in. API collar tools. There are only two circumstances in which the IDD algorithm does not work well. In the first, the tool and borehole are both in gauge, so that the density measurements in all sectors are of equally good quality. The resulting quality factor is a constant with small statistical fluctuations superimposed. Because the tool path is determined by these fluctuations, it jumps randomly around the borehole. In formations with high apparent dip angle, this can lead to erratic densities and depth-matching problems. The preferred density in this case is the

bottom-quadrant density. The second difficult circumstance is more a limitation of the density measurement than of the IDD algorithm itself. It consists of an undergauge tool in a vertical borehole. In this situation, the tool never gets close enough to the borehole wall to make a good density measurement. The IDD algorithm still constructs the best possible density, but its absolute accuracy is poor.

The first example is shown in Figure 4, which presents log data acquired in the Norwegian Sector of the North Sea in a well deviated 25° from the vertical. The top two panels in the figure illustrate the density and quality factor, with the tool path indicated by a thick white line. The tool path clearly follows the center of the quality factor and is roughly one sector to the right of the hole bottom. As seen in the lowest panel, this shift is too small to affect the density values, and the bottom-quadrant and image-derived densities agree completely. These densities are also in agreement with an independent WL log, presented as a thick, dashed line in the figure. Agreement of bottom-quadrant, IDD, and WL densities is seen in many logs in which the tool path lies on the bottom of the borehole and confirms the accuracy of the IDD algorithm's density determination.

Less typical is the situation in Figure 5, which is from an upper section of the same well as the preceding example. The deviation is still 25°. The tool path has drifted farther to the right of the borehole. The origin of this effect may be the competition between the frictional force of the borehole on the rotating tool, causing the tool to move up the side of the borehole, and gravity, which tends to pull the tool to its bottom. The bottom-quadrant and image-derived densities differ by approximately 0.05 g/cm^3 (shaded region in the bottom panel). The WL density is in agreement with the IDD algorithm and not the bottom-quadrant density. The IDD algorithm thus successfully compensates for static displacements of the tool from the hole bottom.

The IDD algorithm also handles dynamic displacements, as seen in Figure 6. This log, from a well in the UK Sector of the North Sea deviated 33° from the vertical, exhibits extreme variability of the tool path. The variability is seen directly in the density. In the zone between 5400 and 5440 ft, the tool path is close to the hole bottom, and the bottom-quadrant and image-derived densities agree. On the other hand, in the zone between 5380 and 5400 ft, the tool path is almost on the top of the hole. The bottom-quadrant and image-derived densities differ by almost 0.2 g/cm^3. Comparison with the densities above and below this zone indicates that the IDD algorithm provides a clearly superior density. Although the correction of density logs affected by a constant shift of the tool path from the bottom, as in the previous example, is relatively easy to do manually from the density image data, the rapidly varying tool motion that occurred in Figure 6 would be extremely time consuming to fix. The IDD algorithm automates this process and gives the highest-quality density in both static and dynamic situations.

Figure 7 shows a log made with an adnVISION475* Azimuthal Density Neutron Vision 475 tool with an in-gauge stabilizer in a nearly horizontal section. As seen in the top two panels of the figure, the density measurements are of high quality over the entire circumference of the borehole. As noted above, this is a particularly challenging situation for the IDD algorithm. One would expect a chaotic tool path and fluctuating density. There are portions of this log that meet that expectation, for example around 4300 ft. But in most of the log, there is sufficient asymmetry in the quality factor to give a density in close agreement with the bottom-quadrant density. Nevertheless, the bottom-quadrant density is the preferred density in this situation.

This example also illustrates one of the limitations of taking the maximum sector density as the highest-quality density. The density image in Figure 7 shows beds of various densities intersecting the wellbore at high apparent dip angles. As seen in the third panel of the figure, the maximum density follows the high-density beds and does not detect the low-density beds. By incorporating several factors besides the apparent density, the IDD algorithm follows the tool path and not the dipping beds.

Another limitation of the maximum density approach is exemplified in the log shown in Figure 8, which is from a well in the Gulf of Mexico deviated 31° from the vertical. The mud weight in this case is very heavy, about 17 to 18 lbm/gal. The density image shows regions of high and low density, but neither is on the hole bottom. The high concentration of barite in the mud causes the *U* factor to be a very sensitive indicator of stand-off, and it dominates the quality factor. The resulting tool path is pinned to the sector with the lowest apparent *U*. Comparing the tool path with the density image, it is clear that the low-density, not the high-density, regions give the highest-quality formation measurements. This interpretation is confirmed in the bottom panel, in which the image-derived Pe is seen to be much lower than the bottom-quadrant Pe. The effect on the density can be enormous, more than 0.6 g/cm^3 at some depths.

The IDD algorithm yields better density values in heavy drilling fluids and heterogeneous formations than a maximum density algorithm. Moreover, by consistently selecting the highest densities from a statistically noisy measurement, the maximum-density approach is biased to high densities by an amount on the order of the precision of the measurement. The IDD algorithm samples all available sectors in computing the tool path and then averages several sectors about the tool path to produce the final density, eliminating this kind of bias.

The IDD algorithm employed so far averages the sector densities that fall within ±45° of the tool path, creating an effective quadrant density. This quadrant density is not generally aligned with the bottom, left, up, and right quadrants labeled in the figures; they are presented for reference only. Understanding this distinction leads to the question: Is a better density obtained from the single sector ("sector IDD" algorithm) or the effective quadrant ("quadrant IDD" algorithm) containing the tool path?

The answer to this question is shown in the second panel from the bottom of Figure 8, which presents both densities. It is apparent that the density obtained from the sector IDD algorithm is noisier than the one from the quadrant IDD algorithm, although the accuracies are similar. The increased noise is an inevitable consequence of the nuclear counting statistics underlying the density measurement. These statistics imply that the repeatability or noise in a nuclear measurement is proportional to the square root of the count rate. By including four times as many sectors in the quadrant IDD algorithm, the count rate is four times higher and the noise two times smaller than those in the sector IDD algorithm. Accuracy does not appear to suffer, and one has the added advantage that the bottom-quadrant and image-derived densities agree exactly when the tool path is on the hole bottom.

Interpretation can also be improved with the IDD algorithm, as shown for a log from offshore Texas in Figure 9. The borehole is deviated 28° from the vertical. As in Figure 5, the tool path is statically shifted from the bottom of the hole, leading to a difference between the image-derived and bottom-quadrant densities. Comparison of these densities with the neutron porosity in the sand zone from X738 to X752 ft defines a neutron/density crossover in the bottom-quadrant density which is absent in the image-derived density. Resistivity confirms that this is a water-bearing zone. The IDD algorithm thus avoids a false hydrocarbon indication that appears in the bottom-quadrant density.

Another example, from a well in West Africa deviated 21° from the vertical, is shown in Figure 10. The natural gamma ray in Track 1 clearly shows a bed boundary at about X835 ft. As the density tool passes through this boundary, the tool path flips entirely around the borehole, as seen from the Pe image in Track 3. The result is that the bottom-quadrant density (Track 2) shows no indication of this bed until the tool path returns to the hole bottom, about 35 ft too deep. The IDD algorithm, on the other hand, places the bed boundary at the correct depth. The image-derived Pe, plotted in Track 2, is also insensitive to this drastic tool motion after X835 ft, whereas the bottom-quadrant Pe gives mistakenly large readings.

SUMMARY

Image-derived density provides the highest-quality formation measurement possible. The algorithm accomplishes this by combining azimuthal data acquisition with an estimate of measurement quality at each depth level and azimuthal sector. From the resulting quality factor, a tool path is identified about which the density and Pe are computed. The IDD algorithm is completely contained within the density sensors and requires no external inputs. From an overlay of the tool path on the density, Pe, or quality factor image and comparison with the bottom-quadrant density, feedback on the reliability of the results is immediately obtained. The algorithm corrects for tool motion in a wide variety of circumstances and provides significant improvements in the accuracy of the density from slick- and stabilized-collar tools. It also addresses many interpretation problems.

ACKNOWLEDGMENTS

The authors thank BP, ChevronTexaco, Kerr-McGee Oil and Gas Corporation, and Statoil for permission to publish the log data presented in this paper.

REFERENCES CITED

Carpenter, W. W., Best, D., and Evans, M., 1997, "Applications and interpretation of azimuthally sensitive density measurements acquired while drilling," *Transactions of the SPWLA 38th Annual Logging Symposium*, Houston, Texas, USA (June), Paper EE.

Ellis, D. V., 1987, *Well Logging for Earth Scientists*, Elsevier, New York, New York, Chapter 10.

Evans, M., Best, D., Holenka, J., Kurkoski, P., and Sloan, W., 1995, "Improved formation evaluation using azimuthal porosity data while drilling," SPE paper 30546, SPE Annual Technical Conference and Exhibition, Dallas, Texas, USA (October).

Radtke, R. J., Adolph, R. A., Climent, H. C., and Ortenzi, L., 2001, "Improved formation evaluation through azimuthal tool-path identification," U.S. Patent Application.

ABOUT THE AUTHORS

R. J. Radtke is presently a senior tool physicist in the nuclear/acoustics discipline for Schlumberger in Sugar Land, Texas. He had post-doctoral appointments at Harvard University and the University of Maryland after graduating from The University of Chicago in 1994 with a PhD in physics. He joined Schlumberger in 1999 at the Sugar Land Product Center, where he is involved in the design of and algorithm development for nuclear logging-while-drilling tools.

R. A. Adolph has worked for 23 years with Schlumberger on engineering teams designing nuclear logging tools for cased hole, openhole wireline, and logging while drilling. Pulsed-neutron and spectroscopy technologies have been a career focus. A graduate of Rice University, he is presently assigned to the Princeton (NJ) Technology Center.

H. C. Climent received a PhD in physics and chemistry of the earth from the European Community in 1996. She worked as a post-doctoral fellow for the Science and Technology Agency at the National Institute of Radiological Sciences in Japan on alpha particle emitters used as tracers. She joined the Schlumberger Sugar Land Product Center in 2000, where she started working on the image-derived density project. She is currently working in the resistivity team.

L. Ortenzi is an LWD interpretation and development engineer for Schlumberger in Stavanger, Norway. Previously, he participated in the development of LWD nuclear answer products at the Schlumberger Sugar Land (TX) Product Center. Since he joined Schlumberger in 1993, he has been involved with LWD interpretation and quality control. He holds an MS degree in geology from the University of Camerino (Italy).

N. Wijeyesekera is formation evaluation business development manager for the Middle Eastern/Asian Area and is based in Dubai, UAE. He graduated from Cornell University in 1992 with a PhD in electrical engineering. He joined Schlumberger immediately afterward and, prior to his current assignment, worked in research and engineering on nuclear, resistivity, and sonic tools in both cased and openhole environments.

P

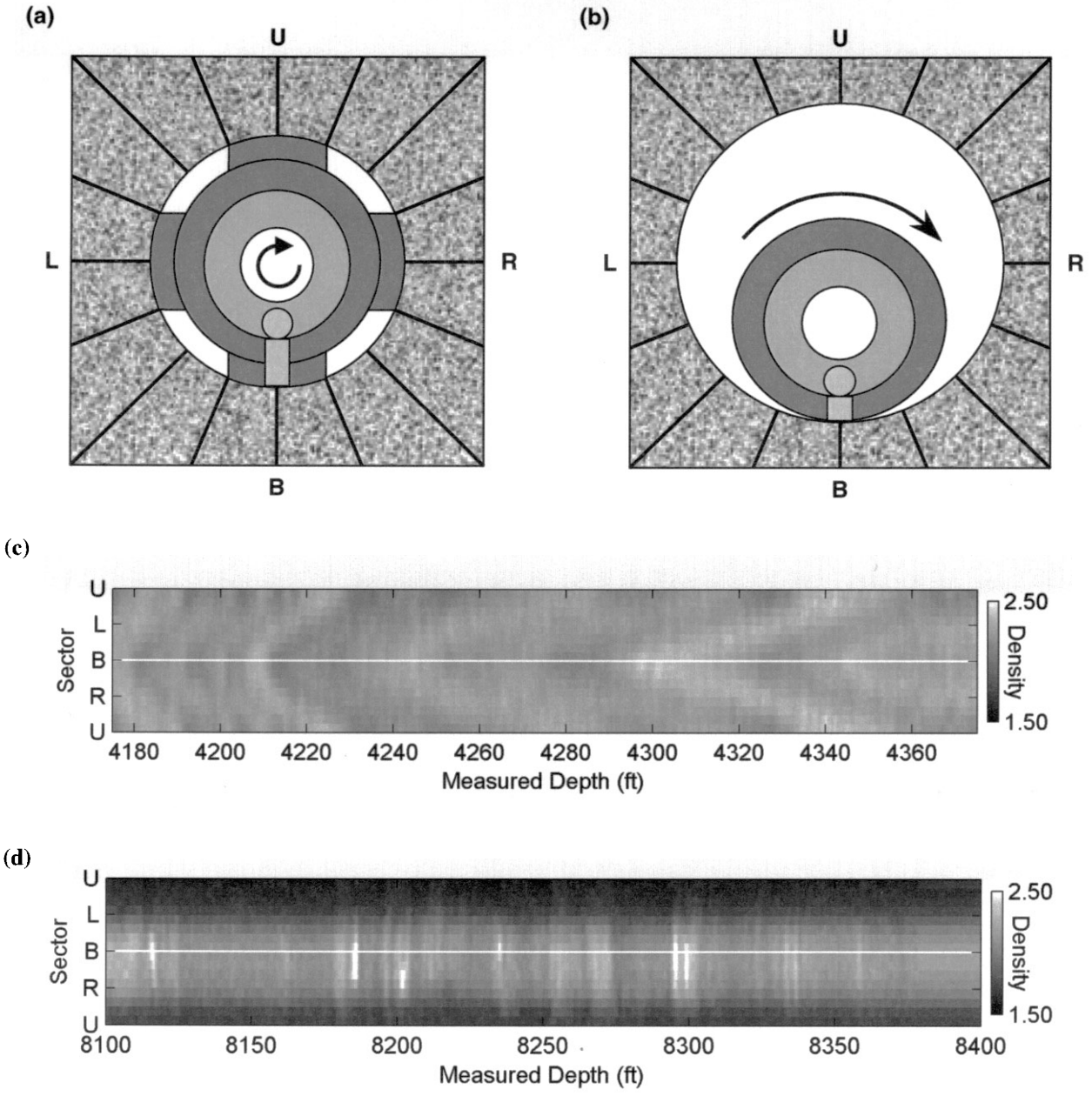

Figure 1: (a) Axial cross section of a stabilized LWD density tool in a deviated borehole. The lightest gray regions are the gamma ray detector and collimator, medium gray is the chassis, and dark gray is the collar and stabilizer. The inner mud channel and borehole are shown in white. The formation surrounds the borehole. As the tool rotates (arrow shows direction), count rate data are binned to the sector in which the density detector is located. The sector boundaries are indicated by black lines in the figure. The sectors are oriented with respect to gravity; bottom (B), left (L), up (U), and right (R) directions are labeled. (b) The same presentation as in (a) but for a slick LWD density tool in a deviated borehole. Typical density images obtained from stabilized and slick tools are shown in (c) and (d), respectively. The white line marks the bottom of the borehole.

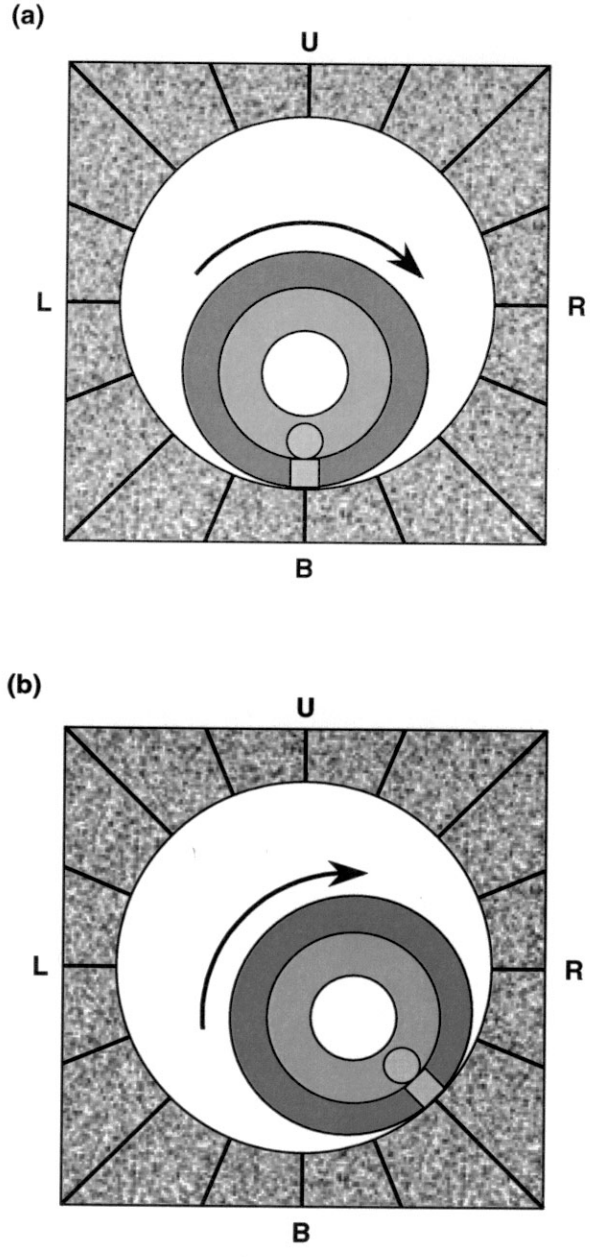

Figure 2: Cross section of a slick or undergauge LWD density tool in a deviated borehole. The color and labeling scheme is as in Figure 1. In (a), gravity causes the tool to settle on the bottom of the borehole, so the highest-quality formation density measurements are derived from the bottom (B) sectors. In (b), the dynamics of the drillstring cause the tool to move to one side of the borehole. The highest-quality formation density measurements are made from the sectors between the bottom (B) and right (R) directions.

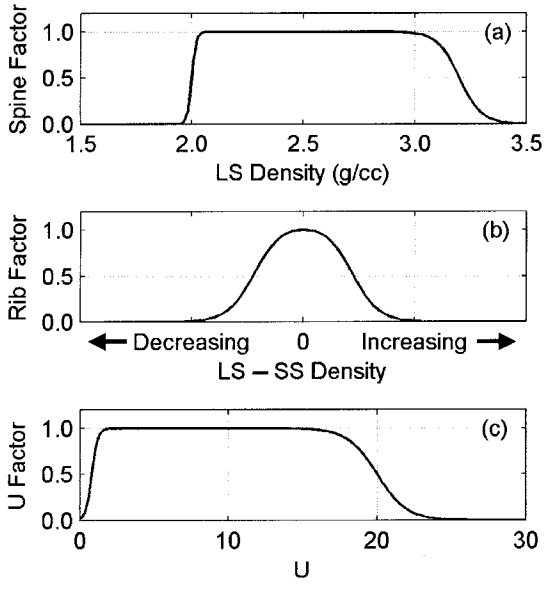

Figure 3: Components of the quality factor. (a) The spine factor as a function of the electron density index from the long-spaced detector, (b) the rib factor as a function of the electron density index difference between long- and short-spaced detectors, and (c) the *U* factor as a function of the volumetric photoelectric factor.

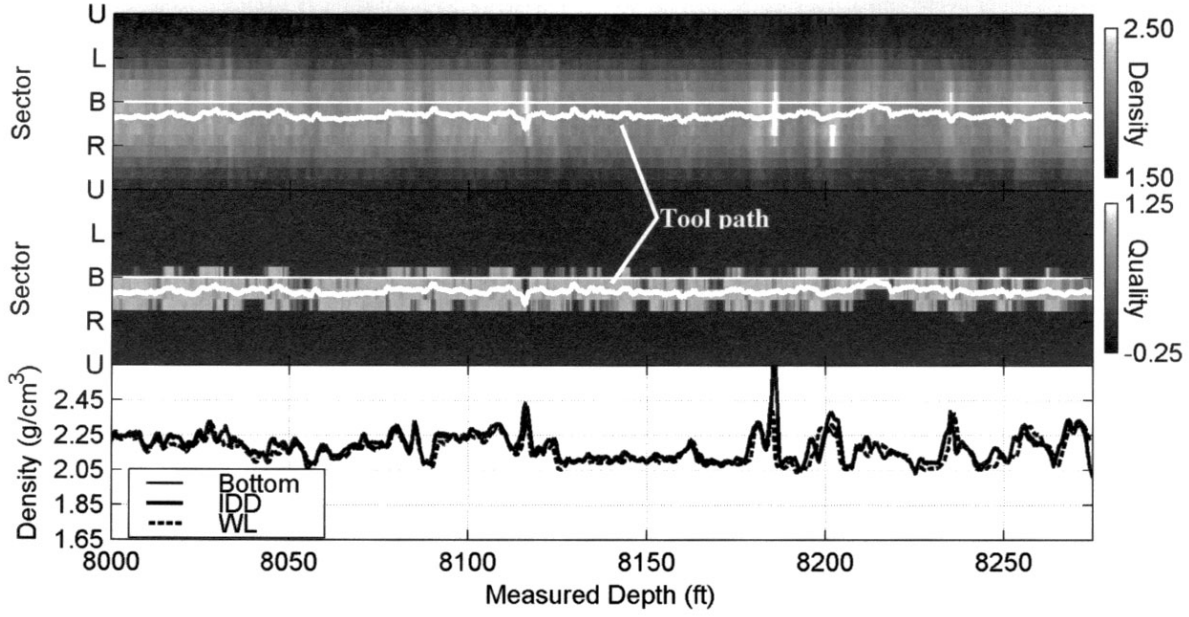

Figure 4: Log from the North Sea demonstrating the equivalence of bottom-quadrant and image-derived densities when the tool path is near the bottom of the hole. The top and middle panels show the oriented density and quality factor images, respectively. In these panels, the thin white line indicates the bottom of the hole, the thick white line is the tool path computed as described in the text, and the up (U), right (R), bottom (B), and left (L) directions are marked. The bottom panel contains the bottom quadrant (thin solid line), image-derived (thick solid line), and wireline (thick dashed line) densities. The borehole is deviated 25° from the vertical.

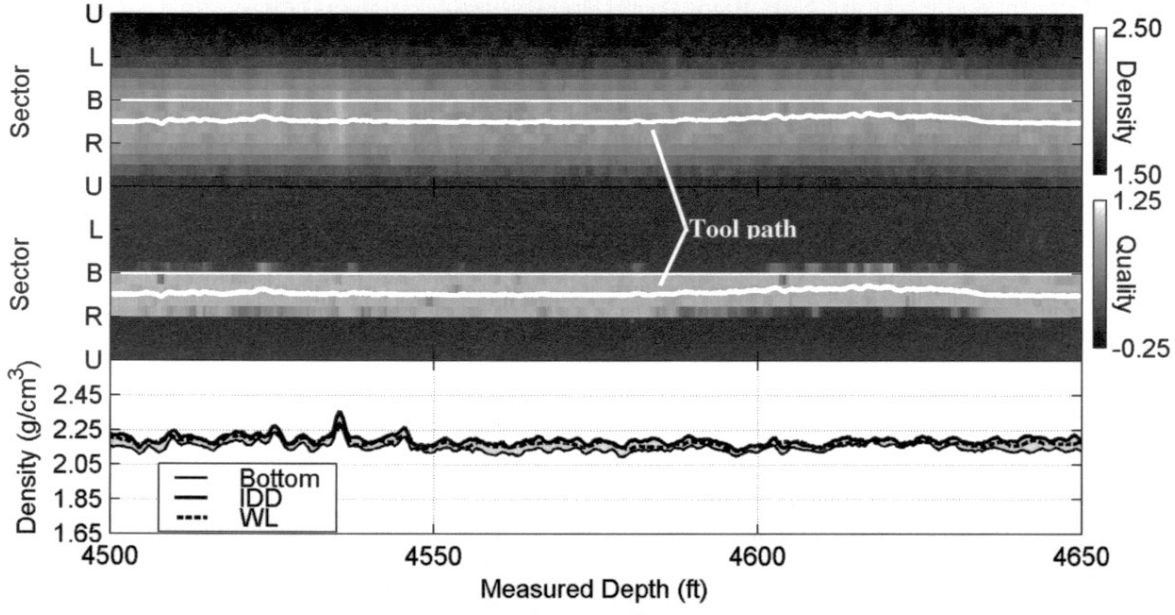

Figure 5: Shallower section of the log from Figure 4 in which a shift of the tool path from the hole bottom causes the bottom-quadrant and image-derived densities to differ significantly (shaded region in bottom panel). In the bottom panel, the wireline density agrees with the image-derived density. The figure format is the same as in Figure 4. The borehole is deviated 25° from the vertical.

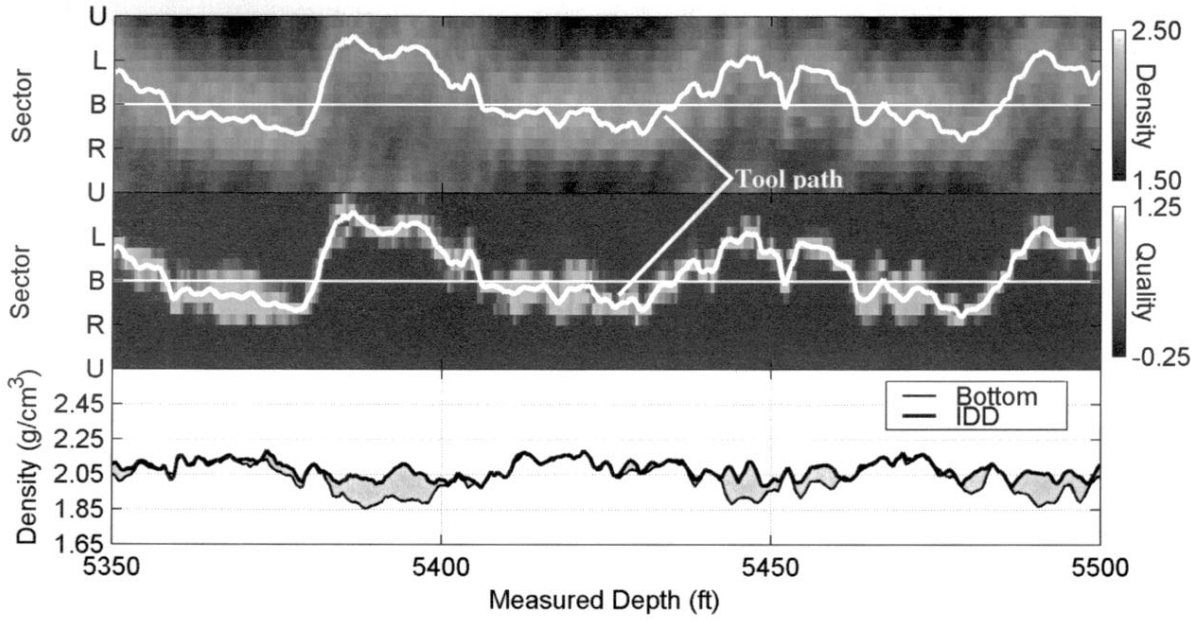

Figure 6: Log from the UK Sector of the North Sea illustrating an erratic tool path. When the path is near the hole bottom, the bottom-quadrant and image-derived densities agree. When the tool path deviates significantly from the bottom, the two densities disagree (shaded regions in the bottom panel). The image-derived density is more accurate in these cases. The figure format is the same as in Figure 4. The borehole is deviated 33° from the vertical.

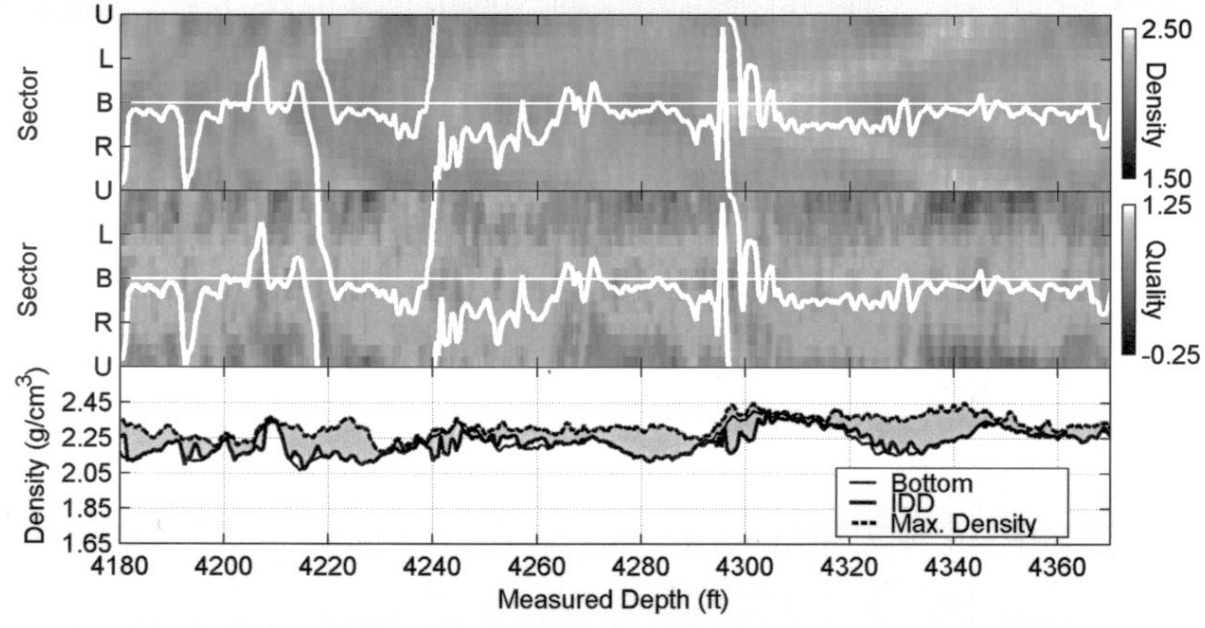

Figure 7: Log in a nearly horizontal well. The top two panels are as in Figure 4. The third panel contains the bottom quadrant (thin solid line), image-derived (thick solid line), and maximum (thick dashed line) densities. The maximum density mistakenly follows the high-density beds and yields erroneously higher densities than the image-derived density (shaded region).

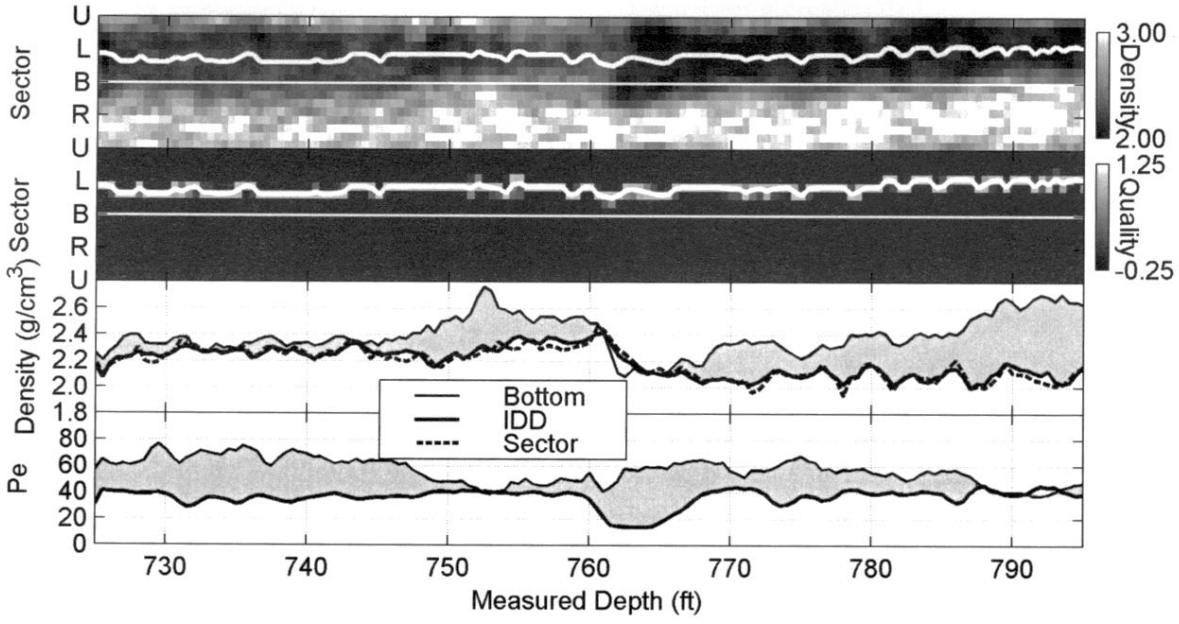

Figure 8: Well from the Gulf of Mexico drilled with heavy drilling fluid. The top two panels are as in Figure 4. The next panel down contains the bottom quadrant (thin solid line), image-derived quadrant (thick solid line), and image-derived sector (thick dashed line) densities. The bottom panel shows the bottom quadrant (thin solid line) and image-derived quadrant (thick solid line) Pe. In this log, the most accurate density is the lower density. The borehole is deviated 31° from the vertical.

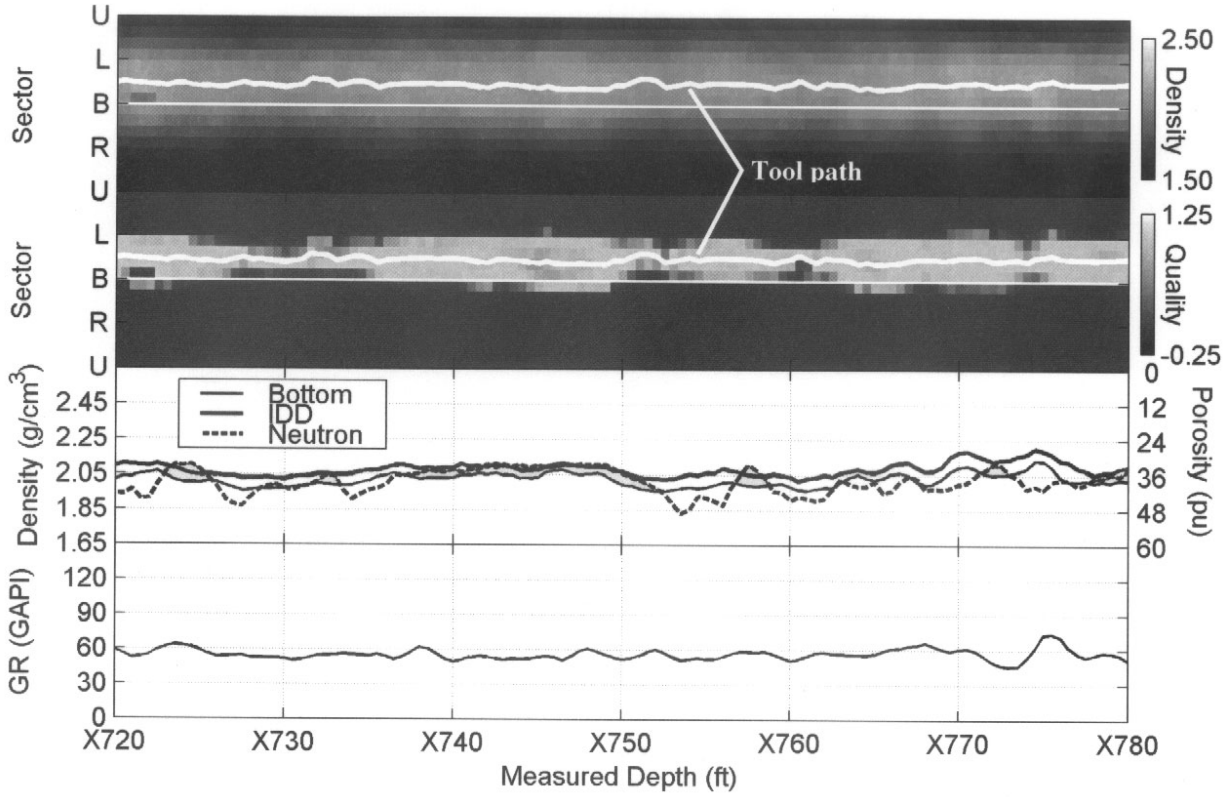

Figure 9: Log from offshore Texas. The top two panels are as in Figure 4. The third panel contains the bottom quadrant (thin solid line) and image-derived (thick solid line) densities along with the neutron porosity in a sandstone matrix (thick dashed line, right-hand scale). The bottom panel displays the natural gamma ray measurement. The tool path is shifted from the hole bottom, causing a difference in the bottom-quadrant and image-derived densities. A hydrocarbon indication seen in the bottom-quadrant neutron/density crossover (shaded region in the third panel) is not present in the image-derived density. The borehole is deviated 28° from the vertical.

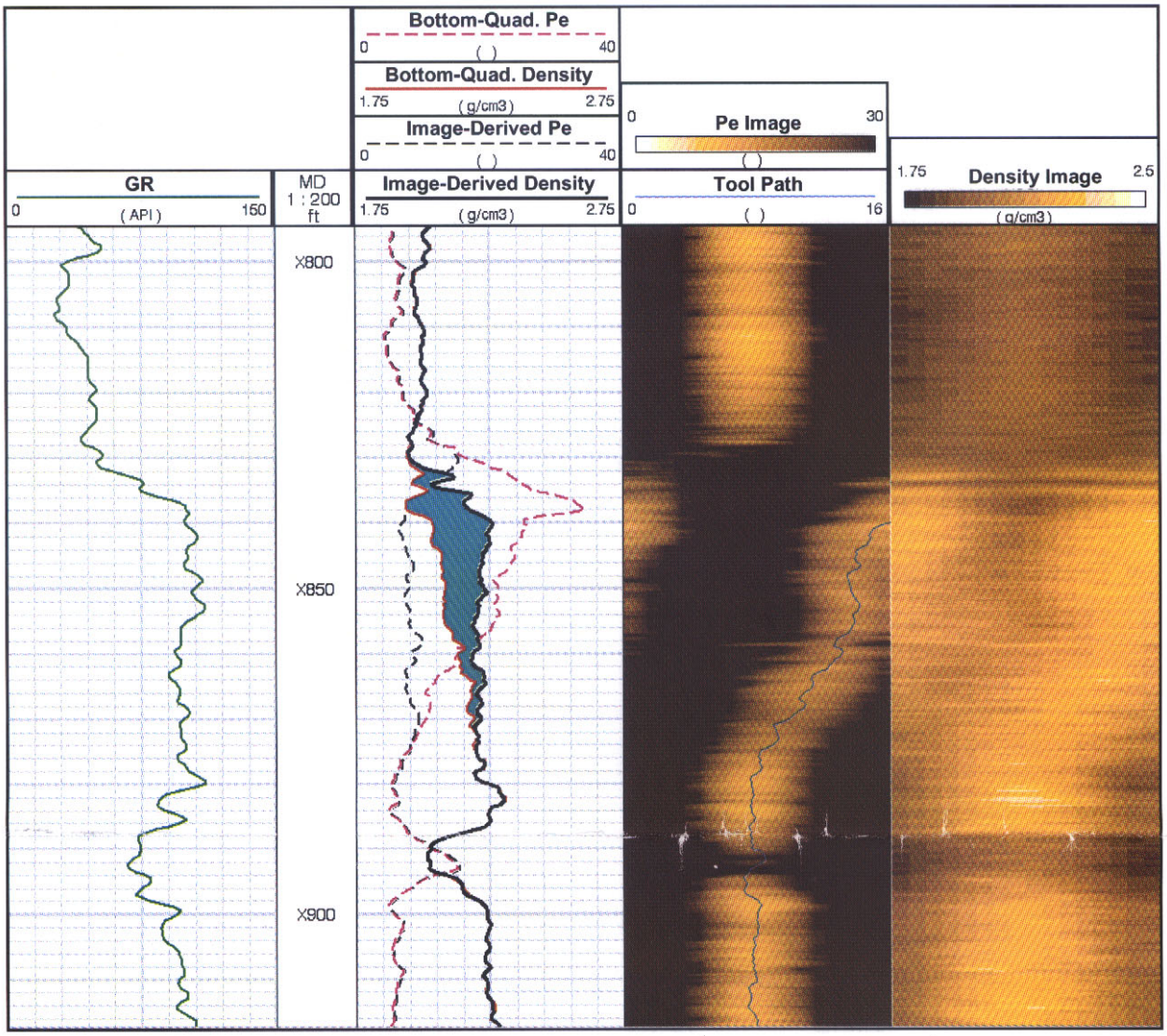

Figure 10: **Log from West Africa showing how the IDD algorithm can improve bed boundary detection. The first track presents the natural gamma ray measurements; the second, bottom-quadrant Pe (dashed magenta line) and density (solid red line) along with image-derived Pe (dashed black line) and density (solid black line); the third, the Pe image and tool path (blue line); and the last, the density image. In track 2, the difference between bottom-quadrant and image-derived densities is shaded green. The bottom quadrant density clearly misses the bed boundary at about X835, but the image-derived density does not. The borehole is inclined 21° from the vertical.**